Solution Process

Masahiro Tatsumisago and Atsushi Sakuda

Abstract Liquid-phase synthesis processes of sulfide-based solid electrolytes can be classified into two categories: suspension processes and solution processes. In the solution process, the precursors of sulfide-based solid electrolytes form homogenous solutions. This chapter summarizes the preparation of sulfide-based solid electrolytes by the solution process. The development of argyrodite solid electrolytes via precursor solution is also shown as a reprehensive of liquid-phase synthesized sulfide-based solid electrolyte with a high conductivity of more than 10^{-3} S cm^{-1} at 25 °C.

Keywords Liquid-phase synthesis · Solid electrolyte · Sulfide · Argyrodite

1 Preparation of Solid Electrolyte via Homogeneous Solution

As described above, liquid-phase synthesis processes can be categorized into two categories: suspension processes [1–20] and solution processes [21–38].

Suspension processes are conducted by stirring the starting materials in organic solvents in which they have low solubility and the precursor particles of solid electrolytes are suspended in the solvents as shown in Chap. 6 "Suspension Process". In the solution process, the precursors of sulfide-based solid electrolytes form homogenous solutions. This process is mainly conducted via a dissolution-precipitation process in which solid electrolytes prepared by solid-state or mechanochemical techniques are dissolved into solvents. Some papers report the preparation of precursor solutions of sulfide-based solid electrolytes solely by a liquid-phase process. Table 1 summarizes the preparation of sulfide-based solid electrolytes by the solution process. Polar solvents such as amides [22–25], alcohols [21, 26–30, 36–38], and

M. Tatsumisago (✉) · A. Sakuda
Osaka Prefecture University, Sakai, Japan
e-mail: tatsu@osakafu-u.ac.jp

A. Sakuda
e-mail: saku@chem.osakafu-u.ac.jp

K. Kanamura (ed.), *Next Generation Batteries*,
https://doi.org/10.1007/978-981-33-6668-8_7

Table 1 Sulfide-based solid electrolytes prepared via homogeneous precursor solution

Electrolyte	Starting material	Solvent	Pre-treatment	Conductivity/S cm^{-1}	Refs.
$Li_{3.25}Ge_{0.25}P_{0.75}S_4$	Li_2S, GeS_2, P_2S_5	Hydrazine	Solid phase	1.8×10^{-4}	[22]
Li_3PS_4	Li_2S, P_2S_5	NMF	Mechanochemical	2.6×10^{-6}	[23]
Li_3PS_4	Li_2S, P_2S_5	NMF, hexane	-	2.3×10^{-6}	[25]
Amorphous Li_3PS_4	Li_2S, P_2S_5, S	DEGDME	-	2.8×10^{-5}	[33]
Li_6PS_5Cl	Li_2S, P_2S_5, LiCl	EtOH	Mechanochemical	1.9×10^{-4}	[36, 37]
Li_6PS_5Cl	Li_2S, P_2S_5, LiCl	EtOH	Mechanochemical	6.0×10^{-4}	[26]
Li_6PS_5Br	Li_2S, P_2S_5, LiBr	EP + EtOH	-	3.4×10^{-5}	[27]
Li_6PS_5Br	Li_2S, P_2S_5, LiBr	THF + EtOH	-	3.1×10^{-3}	[38]
$Li_6PS_5BH_4$	Li_2S, P_2S_5, $LiBH_4$	THF + EtOH	-	1.3×10^{-4}	[28]
Li_4SnS_4	Li_2S, SnS_2	Water	Solid phase	1.4×10^{-4}	[31]
Li_4SnS_4	Li_2S, SnS_2	MeOH	Solid phase	8.9×10^{-5}	[29]
Amorphous LiI-Li_4SnS_4	Li_2S, SnS_2, LiI	MeOH	Solid phase	4.1×10^{-4}	[29]
Na_3PS_4	Na_2S, P_2S_5	NMF	-	2.6×10^{-6}	[39]
Na_3SbS_4	Na_2S, Sb_2S_3, S	MeOH	Solid phase	2.3×10^{-4}	[21]
Na_3SbS_4	Na_2S, Sb_2S_3, S	Water	Solid phase	2.6×10^{-4}	[21]
Na_3SbS_4	Na_2S, Sb_2S_3, S	Water	-	1.2×10^{-3}	[40]
NaI-Na_3SbS_4	Na_2S, Sb_2S_3, S, NaI	MeOH	Solid phase	7.4×10^{-4}	[30]

(continued)

Table 1 (continued)

Electrolyte	Starting material	Solvent	Pre-treatment	Conductivity/S cm^{-1}	Refs.
Na_3SbS_4-Na_4SnS_4	Na_2S, Sb_2S_3, SnS_2, S	Water	Solid phase	3.0×10^{-4}	[32]

water [31, 32] are generally utilized for the solution process. The first report was made by Wang et al. in 2012 [22]; $Li_{3.25}Ge_{0.25}P_{0.75}S_4$ thin film with a conductivity of 1.82×10^{-4} S cm^{-1} was prepared by dissolving the solid electrolyte in hydrazine to form a homogenous solution and subsequent drying at 240 °C. According to a study by Teragawa and Tatsumisago et al., Li_2S-P_2S_5 solid electrolyte having a conductivity of 2.6×10^{-6} S cm^{-1} at room temperature was prepared using *N*-methylformamide (NMF) [23–25]. Sulfide-based solid electrolytes can be dissolved more stably in basic amide solvents than other solvents. Park and Jung et al. demonstrated that a LiI-Li_4SnS_4 solution was obtained by dissolving Li_4SnS_4 synthesized by the solid-phase method and LiI in methanol [29]. Amorphous LiI-Li_4SnS_4 solid electrolytes with a high conductivity of 4.1×10^{-4} S cm^{-1} were synthesized without side reactions because of the high stability of SnS_4^{4-} to oxide ions in nucleophilic solvents.

2 Precursor Solution of Argyrodite Solid Electrolytes

Argyrodite-type solid electrolytes Li_6PS_5X (X = Cl, Br) have been reported to show high conductivity [41–44]. Recently, they were found to be particularly suitable for the solution process [36–38]. Thus, the focus here is on Argyrodite-type solid electrolytes. Some tips on the preparation of Argyrodite-type solid electrolytes are discussed.

Yubuchi et al. produced an ethanol solution of Li_6PS_5Cl by dissolving mechanochemically prepared Li_6PS_5Cl in anhydrous ethanol [36, 37]. Argyrodite Li_6PS_5X electrolytes with high ionic conductivities were also synthesized from Li_2S, P_2S_5, and LiX solely via solution processing using a mixture of tetrahydrofuran and ethanol as the solvent [38]. Scheme 1 shows a schematic illustration of the liquid-phase synthesis of argyrodite-type Li_6PS_5Br and a picture of the obtained precursor solution. The concentrations of Li_6PS_5Br were 5-10 wt%. Figure 1a shows the Raman spectrum for the THF-EtOH precursor solution of Li_6PS_5Br and Li_6PS_5Br solid electrolyte particles prepared by liquid-phase or mechanochemical processes. Raman bands originating from the PS_4^{3-} unit were detected at around 420 cm^{-1} in all the samples, indicating that THF and EtOH did not kinetically decompose the PS_4^{3-} unit. Figure 1b presents XRD patterns of Li_6PS_5Br solid electrolyte particles prepared with different processes and heat treatment temperatures. All the samples consisted of mainly lithium-ion conducting argyrodite Li_6PS_5Br crystals, along with

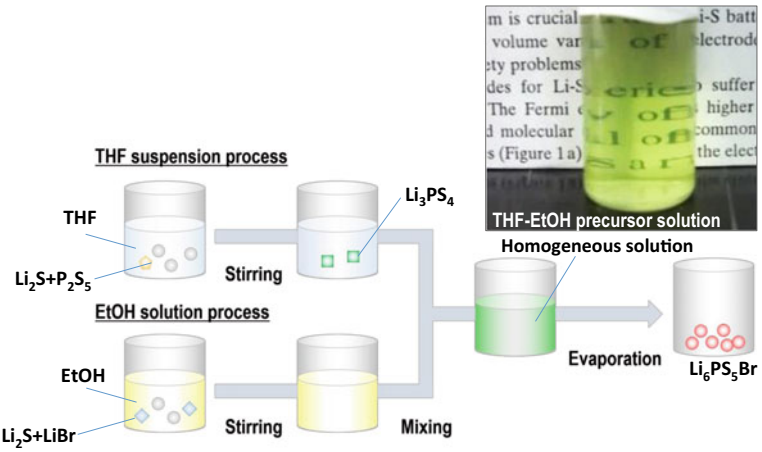

Scheme 1 Schematic illustrations of liquid-phase synthesis of Li_6PS_5Br with both EtOH and THF

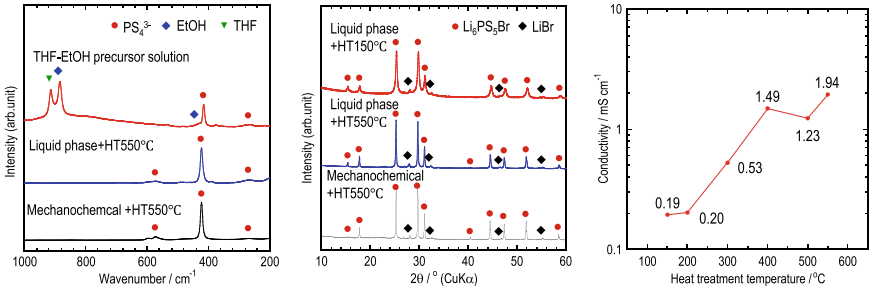

Fig. 1 **a** Raman spectra and **b** XRD patterns of Li_6PS_5Br prepared by liquid-phase process and mechanochemical processes and **c** the conductivities at 25 °C of the green compacts of the argyrodite electrolytes prepared by different heat treatment temperatures

a small amount of LiBr crystals. The crystallinity of Li_6PS_5Br was increased by heat treatment at 550 °C. The Li_6PS_5Br prepared by liquid-phase process and heat treatment at 550°C was confirmed to have the argyrodite structure ($a = 9.9641(2)$ Å, $F3\,m$, (216)) from the powder XRD pattern and the Rietveld refinement analysis technique. Figure 1c shows the conductivities of green compacts (powder compressed pellets) of the solution-synthesized Li_6PS_5Br. Conductivities of over 10^{-3} S cm^{-1} were achieved by heat treatment at 400-550°C. The sintered body at 550 °C showed a high ionic conductivity of 3.1×10^{-3} S cm^{-1}, which is comparable to the conductivity of Li_6PS_5Br prepared by the solid-phase method. These results show that liquid-phase synthesis is a viable candidate for replacing conventional synthetic techniques. Figure 2 summarizes the temperature dependence of the conductivities of liquid-phase prepared solid electrolytes including both suspension and solution processes.

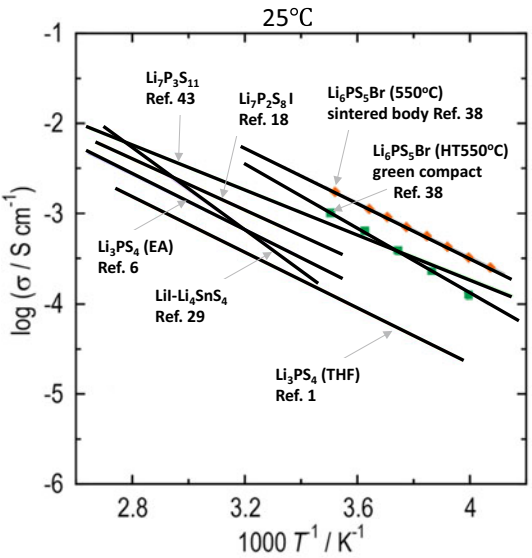

Fig. 2 Arrhenius plots of sulfide-based solid electrolytes prepared by the liquid-phase process. The green compacts were prepared by pressing the obtained powder at room temperature. The sintered body was obtained by heat treatment of the pellet. [1, 6, 18, 29, 38, 45]

Argyrodite Li_6PS_5Br shows higher conductivity than the other solid electrolytes prepared by a liquid-phase process.

Rosero-Navarro et al. reported that the morphology of precipitated particles is controllable by the addition of dispersant [26]. The addition of dispersant produced homogeneous and submicron-sized Li_6PS_5Cl particles while the same conditions without dispersant produced aggregates a few microns in size.

The generation mechanism of the sulfide-based solid electrolytes via solution has not been fully clarified yet. Deeper insight into the mechanism will enable the production of other kinds of sulfide-based solid electrolytes in the future.

References

1. Liu, Z., Fu, W., Payzant, E. A., Yu, X., Wu, Z., Dudney, N. J., et al. (2013). *Journal of the American Chemical Society, 135,* 975–978.
2. Sedlmaier, S. J., Indris, S., Dietrich, C., Yavuz, M., Dräger, C., Von Seggern, F., et al. (2017). *J Chem Mater, 29*(4), 1830–1835.
3. Choi, S., Lee, S., Park, J., Nichols, W. T., & Shin, D. (2018). *Appl Surface Sci., 444,* 10–14.
4. Lim, H.-D., Yue, X., Xing, X., Petrova, V., Gonzalez, M., Liu, H., et al. (2018). *J Mater Chem A, 6,* 7370–7374.
5. Ito, S., Nakakita, M., Aihara, Y., Uehara, T., & Machida, N. (2014). *Journal of Power Sources, 271,* 342–345.
6. Phuc, N. H. H., Morikawa, K., Totani, M., Muto, H., & Matsuda, A. (2016). *Solid State Ionics, 285,* 2–5.
7. Matsuda, A., Muto, H., & Phuc, N. H. H. (2016). *J Jpn Powder Powder Metallurgy, 63*(11), 976–980.

8. Phuc, N. H. H., Totani, M., Morikawa, K., Muto, H., & Matsuda, A. (2016). *Solid State Ionics, 288,* 240–243.
9. Phuc, N. H. H., Morikawa, K., Totani, M., Muto, H., & Matsuda, A. (2017). *Ionics, 23,* 2061–2067.
10. Phuc, N. H. H., Hirahara, E., Morikawa, K., Muto, H., & Matsuda, A. (2017). *Journal of Power Sources, 365,* 7–11.
11. Phuc, N. H. H., Tokuhara, Y., Muto, H., & Matsuda, A. (2017). *Inorganic Chem Front, 4*(10), 1660–1664.
12. Wang, H., Hood, Z. D., Xia, Y., & Liang, C. (2016). *J Mater Chem A, 4,* 8091–8096.
13. Hood, Z. D., Wang, H., Pandian, A. S., Peng, R., Gilroy, K. D., Chi, M., et al. (2018). *Adv Energy Mater, 8*(21), 100014.
14. Calpa, M., Rosero-Navarro, N. C., Miuram, A., & Tadanaga, K. (2017). *RSC Adv, 7*(73), 46499–46504.
15. Xu, R. C., Wang, X. L., Zhang, S. Z., Xia, Y., Xia, X. H., Wu, J. B., et al. (2018). *J Power Sourves, 374,* 107–112.
16. Wang, Y., Lu, D., Bowden, M., Khoury, P. Z. E., Han, K. S., Deng, Z. D., et al. (2018). *Chemistry of Materials, 30,* 990–997.
17. Xu, R. C., Xia, X. H., Wang, Z. L., Gu, C. D., & Tu, J. P. (2016). *Electrochimica Acta, 219,* 235–240.
18. Rangasamy, E., Liu, Z., Gobet, M., Pilar, K., Sahu, G., Zhou, W., et al. (2015). *Journal of the American Chemical Society, 137*(4), 1384–1387.
19. Wan, H., Mwizerwa, J. P., Qi, X., Xu, X., Li, H., Zhang, Q., et al. (2018). *Mater Interfaces, 10,* 12300–12304.
20. Wan, H., Mwizerwa, J. P., Qi, X., Liu, X., Xu, X., Li, H., et al. (2018). *ACS Nano, 12,* 2809–2817.
21. Banerjee, A., Park, K. H., Heo, J. W., Nam, Y. J., Moon, C. K., Oh, S. M., et al. (2016). *Angewandte Chemie Int Ed, 55,* 9634–9638.
22. Wang, Y., Liu, Z., Zhu, X., Tang, Y., & Huang, F. (2013). *Journal of Power Sources, 224,* 225–229.
23. Teragawa, S., Aso, K., Tadanaga, K., Hayashi, A., & Tatsumisago, M. (2013). *Chemistry Letters, 42,* 1435–1437.
24. Teragawa, S., Aso, K., Tadanaga, K., Hayashi, A., & Tatsumisago, M. (2014). *Journal of Power Sources, 248,* 939–942.
25. Teragawa, S., Aso, K., Tadanaga, K., Hayashi, A., & Tatsumisago, M. (2014). *J Mater Chem A, 2,* 5095–5099.
26. Rosero-Navarro, N. C., Miura, A., & Tadanaga, K. (2018). *Journal of Power Sources, 396,* 33–40.
27. Chida, S., Miura, A., Rosero-Navarro, N. C., Higuchi, M., Phuc, N. H. H., Muto, H., et al. (2018). *Ceram. Inter., 44*(1), 742–746.
28. Yubuchi, S., Uematsu, M., Sakuda, A., Hayashi, A., Tatsumisago, M. (2018). *255th ACS National Meeting & Exposition.*
29. Park, K. H., Oh, D. Y., Choi, Y. E., Nam, Y. J., Han, L., Kim, J.-Y., et al. (2016). *Advanced Materials, 288*(9), 1874–1883.
30. Park, K. H., Kim, D. H., Kwak, H., Jung, S. H., Lee, H.-J., Banerjee, A., et al. (2018). *J Mater Chem A, 6,* 17192–17200.
31. Choi, Y. E., Park, K. H., Kim, D. H., Oh, D. Y., Kwak, H. R., Lee, Y.-G., et al. (2017). *Chem Sus Chem, 10*(12), 2605–2611.
32. Heo, J. W., Banerjee, A., Park, K. H., Jung, Y. S., & Hong, S.-T. (2018). *Adv Energy Matet, 8*(11), 1702716.
33. Lim, H.-D., Lim, H.-K., Xing, X., Lee, B.-S., Liu, H., Coaty, C., et al. (2018). *Adv Mater Interfaces, 5,* 1701328.
34. Kim, T. W., Park, K. H., Choi, Y. E., Lee, J. Y., & Jung, Y. S. (2018). *J. Mater. Chem. A, 6,* 840–844.
35. Kim, D. H., Oh, D. Y., Park, K. H., Choi, Y. E., Nam, Y. J., Lee, H. A., et al. (2017). *Nano Letters, 17*(5), 3013–3020.

36. Yubuchi, S., Teragawa, S., Aso, K., Tadanaga, K., Hayashi, A., & Tatsumisago, M. (2015). *Journal of Power Sources, 293,* 941–945.
37. Yubuchi, S., Uematsu, M., Deguchi, M., Hayashi, A., Tatsumisago, M., & Appl, A. C. S. (2018). *Energy Mater, 1*(8), 3622–3629.
38. Yubuchi, S., Uematsu, M., Hotehama, C., Sakuda, A., Hayashi, A., & Tatsumisago, M. (2019). *J Mater Chem A, 7,* 558.
39. Yubuchi, S., Hayashi, A., & Tatsumisago, M., (2015). *Chemistry Letters, 44,* 884–886.
40. Yubuchi, S., Ito, A., Masuzawa, N., Sakuda, A., Hayshi, A. & Tatsumisago, M., (2020). *Journal of Materials Chemistry A, 8*, 1947–1954. https://doi.org/10.1039/C9TA02246E
41. Deiseroth, H.-J., Kong, S.-T., Eckert, H., Vannahme, J., Reiner, C., Zaiß, T., et al. (2008). *Angewandte Chemie Int Ed, 47,* 755–758.
42. Boulineau, S., Courty, M., Tarascon, J.-M., & Viallet, V. (2012). *Solid State Ionics, 221,* 1–5.
43. Deiseroth, H.-J., Maier, J., Weichert, K., Nickel, V., Kong, S.-T., & Reiner, C. (2011). *Anorg Allg Chem, 367,* 1287–1294.
44. Kraft, M. A., Culver, S. P., Calderon, M., Böcher, F., Krauskopf, T., Senyshyn, A., et al. (2017). *Journal of the American Chemical Society, 139*(31), 10909–10918.
45. Yao, X., Liu, D., Wang, C., Long, P., Peng, G., Hu, Y.-S., et al. (2016). *Nano Letters, 16,* 7148–7154.